DALTON
FULL PAPER

First-row transition metal complexes of sterically-hindered amidinates

Joseph A. R. Schmidt and John Arnold *

Department of Chemistry, University of California at Berkeley and Chemical Sciences Division, Lawrence Berkeley National Laboratory, Berkeley, California 94720-1460, USA. E-mail: arnold@socs.berkeley.edu

Received 18th March 2002, Accepted 5th July 2002
First published as an Advance Article on the web 15th August 2002

Complexes of sterically-hindered amidinate ligands with first-row transition metals are described. The amidinate ligands feature bulky terphenyl substituents [2,6-(2,4,6-$Me_3Ph)_2Ph$ or 2,6-(4-$^tBuPh)_2Ph$] attached to the backbone carbon atoms, providing bowl-shaped ligand environments. When employing divalent transition metal halides, bis-amidinate metal complexes are formed exclusively, whereas the use of $Ni(acac)_2$ or CuCl allows access to mono-amidinate species. Additionally, the solid-state structure of one mono-amidinate [(L_{Bu^t})Ni(acac)] and three bis-amidinate complexes [$(L_{Me})_2$M; M = Mn, Co, Ni] are presented.

Introduction

Amidines have been known for many years, being first synthesized in 1858 by the reaction of *N*-phenylbenzimidyl chloride with aniline.[1] With the recent surge in the use of nitrogen-donor ligands for organometallic systems, amidines have seen wide investigation. The amidinate ligand is a monoanionic nitrogen-donor ligand that is characterized by an N–C–N backbone in which π-bonds allow delocalization of the negative charge associated with this ligand (Fig. 1). Each of the

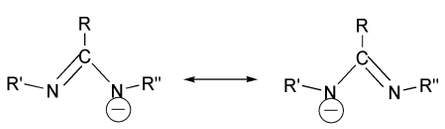

Fig. 1 General form of the amidinate ligand.

three atoms of this backbone has one substituent attached, denoted here by R, R′, and R″ and the ability to modify these three groups allows for tuning of the ligand's electronic and steric environment.

Throughout the course of many studies, coordination of the amidine ligand to virtually every metal in the periodic table has been observed, ranging across the main-group and transition metal series and into the lanthanides.[2] The bis(trimethylsilyl)-benzamidinate ligand (R = Ph; R′ = R″ = $SiMe_3$) has been used extensively because of its easy synthesis, strong binding properties, and the high crystallinity of its compounds.[3–15] More recent work in this area has focused on the use of a wider range of substituents on the amidinate backbone in attempts to tune the electronic and steric properties of this ligand.[16–32] Numerous binding modes have been observed, including simple bidentate coordination to a single metal, monodentate coordination to a single metal center, and coordination to bridge two metal centers. In general, most amidinates are found in the first mode.

A number of studies have focused on the coordination of amidinate ligands to first-row transition metals, with the goal of creating new catalysts having industrial utility.[30–36] Mono-amidinate complexes of di- or tri-valent first-row transition metals appear to be very difficult to synthesize. Rather, bis-amidinate complexes are prevalent in these reactions, regardless of the synthetic pathways employed. As shown in Fig. 2, two

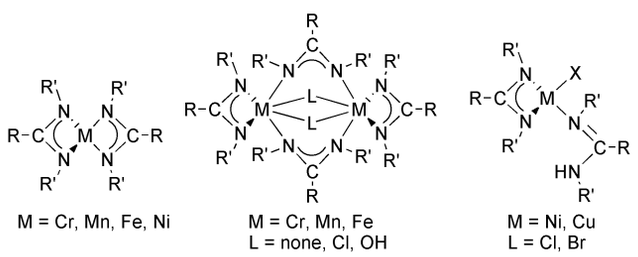

Fig. 2 Common structural motifs found in first-row transition metal amidinate complexes.

structural motifs are prominent: bis-amidinate coordination to a single metal center, and combined bidentate and bridging coordination to a pair of transition metal atoms. Additionally, for trivalent metals, compounds of the form $(amidinate)_3M$ and $(amidinate)_2MX$ are frequently observed, where X = halide. A few known mono-amidinate complexes of first-row transition metals have been formed using monovalent ions, such as Mn(I) and Cu(I) (Fig. 3), by reaction of lithium amidinate with $Mn_2(CO)_8Cl_2$ and $[LCuCl]_2$ starting materials.[37,38]

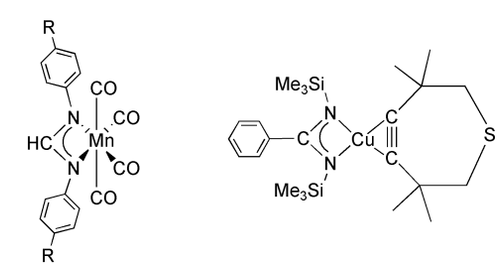

Fig. 3 Mono-amidinate complexes of Mn(I) and Cu(I).

We have previously reported the synthesis and structural properties of a series of amidinate ligands incorporating terphenyl substituents bound to the amidinate carbon atom.[39,40] The terphenyl moieties in these ligands provide steric shielding above and below the plane of the amidinate ligand, creating a bowl-shaped ligand. Through investigation of the free-base and lithium salts of these ligands, it was found that functional groups located at the *ortho* position of the external phenyls of the terphenyl substituents played a strong role in the steric

 DOI: 10.1039/b202737m

effect of these ligands.[39] The large steric bulk of these terphenyl-substituted ligands allowed for the formation of mono-amidinate yttrium halide and amide species, in contrast to the bis-amidinate complexes observed when using less sterically-hindered ligands.[40]

Here, the coordination chemistry of these sterically-hindered amidinates with first-row transition metals is presented. Specifically, reactions forming mono- and bis-amidinate transition metal complexes are detailed. The reactions of the lithium amidinates with divalent metal halides lead exclusively to bis-amidinate metal complexes. By using acetylacetonato (acac) metal complexes or monovalent metal halides, we have been able to prepare mono-amidinate complexes using these sterically-bulky ligands.

Experimental

General considerations

Standard Schlenk-line and glove box techniques were used throughout. Pentane, diethyl ether, and toluene were passed through a column of activated alumina and degassed with argon. THF was passed through a column of activated molecular sieves and degassed with argon. $MnCl_2$, $FeCl_2$, $CoCl_2$, $NiCl_2$, $Ni(acac)_2$, and CuCl were purchased as anhydrous solids, and used as received. $CrCl_2(THF)_2$,[41] L_{Me}–Li(TMEDA),[40] and L_{Bu^t}–Li(TMEDA)[39] were synthesized as detailed previously. C_6D_6 was vacuum transferred from a sodium/benzophenone ketyl. Melting points were determined in sealed capillary tubes under nitrogen and are uncorrected. ^1H and $^{13}C\{^1H\}$ NMR spectra were recorded in C_6D_6 at ambient temperature on a Bruker DRX-500 spectrometer, unless otherwise specified. ^1H NMR chemical shifts are given relative to C_6D_5H (δ 7.16). ^{13}C NMR chemical shifts are relative to C_6D_6 (δ 128.39). IR samples were prepared as Nujol mulls and taken between KBr plates. Magnetic susceptibilities were determined in C_6D_6 using Evans' NMR method.[42] Elemental analyses were determined by the Microanalytical Laboratory of the College of Chemistry, University of California, Berkeley. Mass spectra are from the Mass Spectrometry Laboratory of the College of Chemistry, University of California, Berkeley, and in all cases employed electron impact conditions. Single crystal X-ray structure determinations were performed at CHEXRAY, University of California, Berkeley.

Syntheses

Bis(*N*,*N*′-diisopropyl(2,6-bis-mesityl)benzamidinato)-chromium(II) [$(L_{Me})_2$Cr] (1). A flask containing $CrCl_2(THF)_2$ (300 mg, 1.12 mmol) in THF (30 ml) was cooled to −78 °C, and a solution of L_{Me}–Li(TMEDA) (1.26 g, 2.24 mmol) in THF (40 ml) was added *via* cannula. After a rapid color change to green, the solution was stirred and slowly warmed to room temperature overnight. The solvent was removed *in vacuo*, pentane (40 ml) was added, and the solvent was again removed under vacuum. The solid was extracted with two portions of pentane (40, 20 ml) and the combined extracts were concentrated to 25 ml and cooled to −40 °C. The resulting red crystals were isolated by filtration and dried under vacuum; (298 mg, 29%); mp 242–243 °C; μ_{eff} = 4.65 μ_B; MS: *m*/*z* 931 (M^+); IR: 1611 (m), 1570 (w), 1420 (s), 1356 (s), 1344 (s), 1301 (w), 1255 (w), 1212 (m), 1185 (w), 1163 (w), 1146 (m), 1106 (w), 1030 (w), 995 (m), 849 (s), 815 (w), 776 (s), 752 (w), 721 (w), 656 (w) cm^{-1}. Anal. calc. for $C_{62}H_{78}N_4Cr$: C, 79.96; H, 8.44; N, 6.02. Found: C, 79.57; H, 8.69; N, 5.70%.

Bis(*N*,*N*′-diisopropyl(2,6-bis-mesityl)benzamidinato)-manganese(II) [$(L_{Me})_2$Mn] (2). A reaction flask charged with $MnCl_2$ (67 mg, 0.53 mmol) and THF (20 ml) was cooled to −78 °C and a solution of L_{Me}–Li(TMEDA) (600 mg, 1.07 mmol) in THF (30 ml) was added *via* cannula. The solution was stirred and slowly warmed to room temperature overnight with a color change to a tan-brown hue. The solvent was removed under vacuum, pentane (30 ml) was added, and the volatile fraction was again removed *in vacuo*, yielding a sticky tan-brown solid. The solid was extracted with pentane (40 ml), and the extract was filtered and concentrated to saturation. Cooling to −30 °C yielded the product as a tan microcrystalline solid. After filtration, the product was dried under vacuum; (251 mg, 50%); mp 205–207 °C; μ_{eff} = 5.70 μ_B; MS: *m*/*z* 933 (M^+); IR: 2360 (w), 2342 (w), 1609 (w), 1561 (w), 1484 (w), 1426 (s), 1308 (m), 1224 (w), 1135 (w), 1101 (w), 1029 (w), 1001 (w), 849 (m), 772 (m), 738 (w), 590 (w), 580 (w), 499 (w), 458 (w) cm^{-1}. Anal. calc. for $C_{62}H_{78}N_4Mn$: C, 79.71; H, 8.41; N, 6.00. Found: C, 79.92; H, 8.33; N, 6.05%.

Bis(*N*,*N*′-diisopropyl(2,6-bis-mesityl)benzamidinato)iron(II) [$(L_{Me})_2$Fe] (3). A flask was charged with $FeCl_2$ (56 mg, 0.44 mmol) and THF (20 ml) was added, forming a suspension. The flask was cooled to −78 °C and a solution of L_{Me}–Li(TMEDA) (500 mg, 0.89 mmol) in THF (50 ml) was added slowly *via* cannula. The pale yellow solution was stirred overnight while slowly warming to room temperature. After removal of solvent under vacuum, pentane (30 ml) was added to the sticky solid and the reaction mixture was again pumped down to a solid. The solid was extracted with pentane (50 ml), resulting in a pale yellow solution. This was concentrated slightly under vacuum and then cooled to −30 °C. Large yellow crystals grew over a period of one week at this temperature. The yellow crystals were isolated by filtration and dried under vacuum. The supernatant solution yielded a second crop of crystalline material similarly. The crystals were found to desolvate, forming a tan powder over a few days; (197 mg combined, 47%); mp 178 °C (dec.); μ_{eff} = 4.92 μ_B; MS: *m*/*z* 935 (M^+); IR: 1610 (m), 1563 (w), 1485 (m), 1422 (s), 1309 (s), 1261 (w), 1222 (m), 1183 (w), 1165 (w), 1135 (m), 1101 (m), 1028 (m), 999 (m), 931 (w), 850 (s), 771 (s), 739 (m) cm^{-1}. Anal. calc. for $C_{62}H_{78}N_4Fe$: C, 79.63; H, 8.41; N, 5.99. Found: C, 79.65; H, 8.35; N, 6.12%.

Bis(*N*,*N*′-diisopropyl(2,6-bis-mesityl)benzamidinato)cobalt(II) [$(L_{Me})_2$Co] (4). A suspension of $CoCl_2$ (150 mg, 1.16 mmol) in THF (20 ml) was cooled to −78 °C, and a solution of L_{Me}–Li(TMEDA) (1.3 g, 2.3 mmol) in THF (60 ml) was added *via* cannula. After rapidly changing to a forest green solution, the mixture was stirred while slowly warming to ambient temperature over a period of 14 h. The solvent was removed under vacuum, and pentane (50 ml) was added; this was stirred for 15 min and the solvent was again removed *in vacuo*. The resulting green solid was extracted with two portions of pentane (50, 25 ml), and the combined extracts were concentrated to 15 ml. The solution was cooled to −40 °C, producing green crystals, which were filtered and dried under vacuum. A second crop could be isolated similarly from the supernatant solution; (655 mg combined, 60%); mp 178 °C (dec.); μ_{eff} = 4.73 μ_B; MS: *m*/*z* 937 (M^+); IR: 1609 (w), 1563 (w), 1426 (s), 1311 (m), 1261 (w), 1228 (m), 1183 (w), 1165 (w), 1137 (w), 1103 (m), 1029 (m), 1002 (m), 850 (m), 800 (w), 771 (m), 738 (w), 589 (w), 581 (w), 508 (w), 455 (w) cm^{-1}. Anal. calc. for $C_{62}H_{78}N_4Co$: C, 79.37; H, 8.38; N, 5.97. Found: C, 79.39; H, 8.47; N, 5.86%.

Bis(*N*,*N*′-diisopropyl(2,6-bis-mesityl)benzamidinato)nickel(II) [$(L_{Me})_2$Ni] (5). A reaction flask was charged with $NiCl_2$ (60 mg, 0.46 mmol) and THF (20 ml) and cooled to −78 °C. A solution of L_{Me}–Li(TMEDA) (521 mg, 0.93 mmol) was added *via* cannula and the reaction mixture was stirred overnight while warming to ambient temperature. The solvent was removed under vacuum to yield a red oil. After treatment with pentane (20 ml), the solvent was again removed under vacuum to yield a red solid. This solid was extracted with pentane (30 ml), and the extract was concentrated to 7 ml. Cooling this solution to −30 °C yielded red crystals; (79 mg, 19%); mp 170 °C (dec.);

Table 1 Crystal data and collection parameters

Compound	**2**	**4**	**5**	**7**·1/2C_5H_{12}
Formula	$C_{62}H_{78}N_4Mn$	$C_{62}H_{78}N_4Co$	$C_{62}H_{78}N_4Ni$	$C_{40.5}H_{56}N_2NiO_2$
Formula weight	934.26	938.26	938.03	661.60
Space group	*C*2/*c* (no. 15)	$P2_1/m$ (no. 11)	$P2_1/m$ (no. 11)	$P2_1/c$ (no. 14)
Crystal system	Monoclinic	Monoclinic	Monoclinic	Monoclinic
T/°C	−106	−131	−80	−133
a/Å	15.9920(5)	12.4890(5)	12.459(1)	11.344(2)
b/Å	15.6524(2)	15.8629(7)	15.941(1)	32.816(7)
c/Å	25.7702(7)	14.0309(6)	14.070(1)	10.441(2)
β/°	98.003(2)	105.818(1)	105.396(1)	99.938(3)
V/Å^3	6387.8(2)	2674.4(2)	2694.2(3)	3828(1)
Z	4	2	2	4
Diffractometer	Siemens SMART	Siemens SMART	Siemens SMART	Siemens SMART
Radiation	Mo-Kα (*λ* = 0.71069 Å)	Mo-Kα (*λ* = 0.71069 Å)	Mo-Kα (*λ* = 0.71069 Å)	Mo-Kα (*λ* = 0.71069 Å)
Monochromator	Graphite	Graphite	Graphite	Graphite
Detector	CCD area detector	CCD area detector	CCD area detector	CCD area detector
Scan type, width	*ω*, 0.3°	*ω*, 0.3°	*ω*, 0.3°	*ω*, 0.3°
Scan speed	30.0 s/frame	10.0 s/frame	10.0 s/frame	20.0 s/frame
Reflections measured	Hemisphere	Hemisphere	Hemisphere	Hemisphere
μ/cm^{-1}	2.42	3.63	4.02	5.41
Crystal dimensions/mm	0.31 × 0.14 × 0.07	0.34 × 0.24 × 0.13	0.44 × 0.35 × 0.32	0.26 × 0.21 × 0.13
Reflections measured	13465	12040	13053	17406
Unique reflections	4783	4641	4960	6551
Observations	2506	2534	3086	2987
Parameters	255	343	334	421
R, R_w, R_{all}	0.102, 0.137, 0.156	0.040, 0.042, 0.081	0.035, 0.041, 0.062	0.035, 0.040, 0.095

μ_{eff} = 2.98 μ_B; MS: *m*/*z* 937 (M^+); IR: 1609 (m), 1562 (w), 1423 (s), 1311 (s), 1261 (w), 1229 (m), 1183 (w), 1166 (w), 1137 (m), 1103 (m), 1029 (m), 1002 (m), 932 (w), 850 (s), 820 (w), 772 (s), 737 (w), 588 (w), 580 (w) cm^{-1}. Anal. calc. for $C_{62}H_{78}N_4Ni$: C, 79.39; H, 8.38; N, 5.97. Found: C, 79.07; H, 8.51; N, 5.86%.

(*N*,*N*′-Diisopropyl(2,6-bis-mesityl)benzamidinato)(acetylacetonato)nickel(II) [(L_{Me})Ni(acac)] (6). THF (20 ml) was added to a flask containing Ni(acac)$_2$ (230 mg, 0.90 mmol), forming a dark green suspension. A solution of L_{Me}–Li(TMEDA) (0.50 g, 0.89 mmol) in THF (50 ml) was added slowly *via* cannula, resulting in the immediate formation of pale brown precipitate. The solution was stirred for 14 h at ambient temperature, and then the volatile materials were removed under vacuum to yield a brown material. Pentane (35 ml) was added, the mixture was stirred, and the volatiles were again removed *in vacuo*. Extraction with pentane (3 × 25 ml) yielded a pale green solution, which was pumped down to a green oil that thickened over a period of 1 week. This oil, though contaminated with the free-base ligand L_{Me}H,[40] was mostly the desired product, **6**; (253 mg, 47%); MS: *m*/*z* 597 (M^+); IR: 1665 (m), 1646 (w), 1613 (s), 1598 (s), 1516 (s), 1411 (w), 1399 (s), 1358 (w), 1313 (w), 1259 (m), 1181 (w), 1169 (w), 1127 (w), 1116 (w), 1029 (w), 1015 (m), 957 (w), 920 (w), 849 (m), 801 (m), 762 (m), 753 (w), 742 (w) cm^{-1}.

(*N*,*N*′-Diisopropyl(2,6-bis(4-*tert*-butylphenyl))benzamidinato)(acetylacetonato)nickel(II) [(L_{Bu^t})Ni(acac)] (7). A solution of L_{Bu^t}–Li(TMEDA) (2.5 g, 4.2 mmol) in THF (75 ml) was added to a slurry of Ni(acac)$_2$ (1.09 g, 4.24 mmol) in THF (200 ml), resulting in a dark purple solution. After stirring for 3 h, the volatile materials were removed under vacuum. The resulting solid was extracted with three portions of pentane (200, 50, 50 ml), which were filtered through Celite and combined. The resulting solution was concentrated to saturation and cooled to −30 °C, and large purple crystals grew on standing at this temperature. The crystals were isolated by filtration and dried under vacuum. A second crop could be isolated from the supernatant solution similarly; (1.21 g combined, 46%); mp 235 °C (dec.); ^{1}H NMR *δ* 8.058 (d, 4H, 8 Hz), 7.709 (d, 4H, 8 Hz), 7.346 (d, 2H, 8 Hz), 7.200 (t, 1H, 8 Hz), 4.647 (s, 1H), 2.338 (sept, 2H, 6 Hz), 1.310 (s, 18H), 1.274 (s, 6H), 0.748 (d, 12H, 6 Hz); ^{13}C NMR *δ* 185.5, 171.1, 151.3, 142.5, 139.1, 130.1, 130.0, 129.9, 126.4, 101.0, 45.1, 35.0, 31.8, 25.3, 23.8; MS: *m*/*z* 624 (M^+); IR: 1577 (s), 1523 (s), 1476 (s), 1452 (s), 1391 (s), 1360 (m), 1334 (w), 1307 (w), 1290 (w), 1262 (w), 1240 (m), 1201 (w), 1191 (w), 1167 (w), 1153 (w), 1131 (w), 1113 (m), 1100 (m), 1020 (m), 1009 (m), 844 (w), 830 (w), 807 (m), 777 (m) cm^{-1}. Anal. calc. for $C_{38}H_{50}N_2O_2Ni$: C, 72.97; H, 8.06; N, 4.48. Found: C, 72.62; H, 8.03; N, 4.47%.

(*N*,*N*′-Diisopropyl(2,6-bis(4-*tert*-butylphenyl))benzamidinato)-copper(I) [(L_{Bu^t})Cu]$_x$ (8). A reaction flask was charged with CuCl (750 mg, 7.58 mmol) and THF (25 ml) was added, forming a suspension. A solution of L_{Bu^t}–Li(TMEDA) (3.0 g, 5.1 mmol) in THF (75 ml) was added *via* cannula. After stirring for 14 h, the solvent was removed from the reaction mixture under vacuum, giving a cream-colored solid. The solid was washed with diethyl ether (70 ml) and was then extracted with toluene (150 ml). After filtration through Celite, the solvent was removed *in vacuo* and the product collected as a white solid; (1.234 g, 46%); mp 281 °C (dec.); ^{1}H NMR *δ* 8.034 (d, 4H, 8.4 Hz), 7.537 (d, 2H, 7.6 Hz), 7.465 (d, 4H, 8.4 Hz), 7.253 (t, 1H, 7.6 Hz), 3.327 (sept, 2H, 6.0 Hz), 1.314 (s, 18H), 0.818 (d, 12H, 6.0 Hz); ^{13}C NMR *δ* 171.4, 150.5, 139.9, 138.2, 134.0, 130.1, 129.4, 128.5, 125.2, 49.4, 34.5, 31.5, 27.2; IR: 1611 (w), 1576 (w), 1513 (m), 1487 (s), 1341 (m), 1271 (m), 1167 (w), 1127 (m), 1099 (w), 1020 (w), 1007 (w), 837 (w), 804 (m), 777 (m), 727 (w), 685 (w), 576 (m) cm^{-1}. Anal. calc. for $C_{33}H_{43}N_2Cu$: C, 74.61; H, 8.16; N, 5.27. Found: C, 74.76; H, 7.98; N, 5.01%.

X-Ray crystallography

A summary of crystal data and collection parameters for the crystal structures of **2**, **4**, **5**, and **7** are given in Table 1. Details of individual data collection and solution are given below. ORTEP diagrams were created using the ORTEP-3 software package.[43] For each sample, a crystal was mounted on a glass capillary using Paratone-N hydrocarbon oil. The crystal was transferred to a Siemens SMART[44] diffractometer/CCD area detector, centered in the X-ray beam, and cooled using a nitrogen-flow low-temperature apparatus that had been previously calibrated by a thermocouple placed at the same position as the crystal. A least-squares refinement on data from 60 sample frames allowed determination of cell constants and the orientation matrix. An arbitrary hemisphere of data was collected using 0.3° *ω*-scans, and the data were integrated by

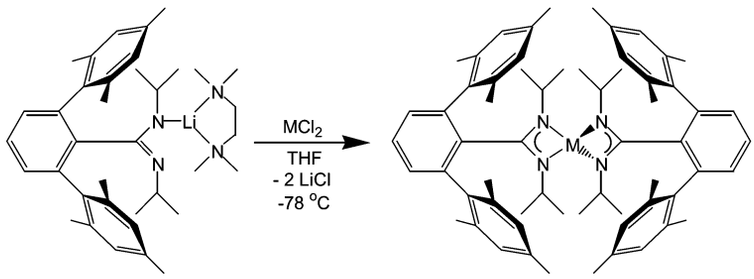

Scheme 1

the program SAINT.[45] The final unit cell parameters were determined by least-squares analysis of the reflections with $I > 10\sigma(I)$. Data analysis using Siemens XPREP[46] determined the space group. The data were corrected for Lorentz and polarization effects, but no correction for crystal decay was applied. Equivalent reflections were averaged, and the structure was solved by direct methods[47] and expanded using Fourier techniques,[48] all within the teXsan[49] software package. The non-hydrogen atoms were refined anisotropically. Hydrogen atoms were included as fixed atoms but not refined. The weighting schemes were based on counting statistics and included a factor ($p = 0.030$) to reduce the weight of intense reflections. The analytical forms of the scattering factor tables for the neutral atoms were used,[50] and all scattering factors were corrected for both the real and imaginary components of anomalous dispersion.[51]

(2). X-Ray quality crystals were grown from a saturated pentane solution that was cooled to −40 °C. The crystal structure of this compound is isomorphic to that found for $(L_{Me})_2Mg$, and has the same two-fold ligand disorder (see previous report).[39] Similarly to $(L_{Me})_2Mg$, the core of the compound is ordered and non-hydrogen atoms in this region were refined anisotropically, while the carbon atoms of the disordered terphenyl moiety were refined isotropically. Many of the hydrogen atoms were included as fixed atoms and not refined. The final cycle of full-matrix least squares refinement (minimizing the quantity $\Sigma w(|F_o| - |F_c|)^2$, where w is the weight of a given observation) was based on 2506 observed reflections [$I > 3.00\sigma(I)$] and 255 variable parameters and converged yielding final residuals:[52] $R = 0.102$, $R_w = 0.137$, and GOF = 4.41.

(4). X-Ray quality crystals were grown from a saturated pentane solution that was cooled to −40 °C. The final cycle of full-matrix least squares refinement (minimizing the quantity $\Sigma w(|F_o| - |F_c|)^2$, where w is the weight of a given observation) was based on 2534 observed reflections [$I > 3.00\sigma(I)$] and 343 variable parameters and converged yielding final residuals:[52] $R = 0.040$, $R_w = 0.042$, and GOF = 1.21.

(5). X-Ray quality crystals were grown from a saturated pentane solution that was cooled to −30 °C. The final cycle of full-matrix least squares refinement (minimizing the quantity $\Sigma w(|F_o| - |F_c|)^2$, where w is the weight of a given observation) was based on 3086 observed reflections [$I > 3.00\sigma(I)$] and 334 variable parameters and converged yielding final residuals:[52] $R = 0.035$, $R_w = 0.041$, and GOF = 1.38.

(7). X-Ray quality crystals were grown from a saturated pentane solution that was cooled to −30 °C. A molecule of pentane is incorporated in the unit cell and resides on an inversion center, causing it to be disordered over two positions. The final cycle of full-matrix least squares refinement (minimizing the quantity $\Sigma w(|F_o| - |F_c|)^2$, where w is the weight of a given observation) was based on 2987 observed reflections [$I > 3.00\sigma(I)$] and 421 variable parameters and converged yielding final residuals:[52] $R = 0.035$, $R_w = 0.040$, and GOF = 1.17.

CCDC reference numbers 182078–182081.

See http://www.rsc.org/suppdata/dt/b2/b202737m/ for crystallographic data in CIF or other electronic format.

Results and discussion

The reactions detailed here are focused on the mesityl-substituted amidinate ($L_{Me}H$) for two main reasons: first, its unique free-base and lithium amidinate geometry indicated the presence of a strong steric effect produced by this ligand;[40] second, the mesityl substituents provided favorable solubility properties. The ^{i}Pr-phenyl substituted amidinate ($L_{Pr}H$) proved to be too soluble, hampering isolation of clean metal complexes in most cases.

Bis-amidinate complexes of first-row transition metals

The lithium amidinate L_{Me}–Li(TMEDA) was found to react readily with divalent first-row transition metal (Cr, Mn, Fe, Co, and Ni) halides. Two equivalents of L_{Me}–Li(TMEDA) reacted with MX_2 in THF at −78 °C to yield bis-amidinate metal complexes in which both halide ligands were substituted by amidinate ligands (Scheme 1). The resulting metal complexes [$(L_{Me})_2M$; M = Cr (**1**), Mn (**2**), Fe (**3**), Co (**4**), and Ni (**5**)] were highly soluble in pentane and were isolated in moderate yields as crystalline compounds. Each of these compounds is paramagnetic and shows broad resonances in its ^{1}H NMR spectrum. In all five cases, the mass spectrum (EI mode) showed a M^+ peak corresponding to the $(L_{Me})_2M$ molecular ion. Using Evans' NMR method,[42] the magnetic susceptibilities of this series of complexes was determined, and all values were characteristic of high-spin metal(II) species. Additionally, the IR spectra of these compounds, though not readily interpretable, were very similar across this series of five compounds. From these data, each compound (**1**–**5**) was assigned a tetrahedral coordination geometry at the metal center composed of the four donor nitrogen atoms from the two amidinate ligands coordinated to the metal center.

Interestingly, although a wide variety of reaction conditions were tested, the bis-amidinate complexes (**1**–**5**) were the only isolable complexes formed. Varying the solvent and the temperature of the reactions did not result in formation of other products. Additionally, reaction of the metal halides with one equivalent of the amidinate [L_{Me}–Li(TMEDA)] only led to the formation of the bis-amidinate species. Moreover, addition of strong donor ligands, such as pyridine or phosphines, also did not prevent formation of the bis-amidinate complexes in these reactions.

In order to confirm the geometry of these bis-amidinate complexes, X-ray quality crystals of some of these species were grown. The crystals of the manganese complex, $(L_{Me})_2Mn$ (**2**), were found to be suitable for X-ray crystallography and the solid-state structure of this compound was determined. The structure is analogous to that observed for $(L_{Me})_2Mg$,[39] exhibit-

ing the same two-fold ligand disorder observed in that system. The amidinate core of the molecule was ordered and the bond lengths and angles associated with this region of the crystallographic model are well determined. On the other hand, positions of the atoms comprising the disordered terphenyl group have a much higher degree of uncertainty. The crystal structure of **2** confirms the tetrahedral geometry of this bis-amidinate complex and the ordered portion of the molecule is shown in Fig. 4, along with selected bond lengths and angles. In

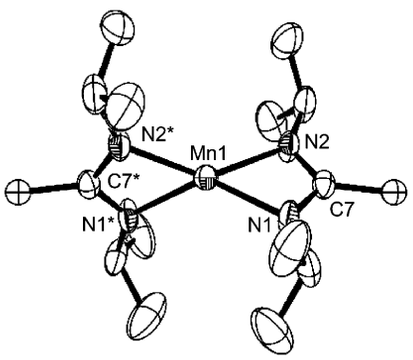

Fig. 4 ORTEP view of the ordered core of $(L_{Me})_2Mn$ (**2**) with 50% thermal ellipsoids. Selected bond lengths (Å): Mn1–N1 = 2.096(7), Mn1–N2 = 2.075(7), N1–C7 = 1.33(1), N2–C7 = 1.34(1); bond angles (°): N1–Mn1–N2 = 63.3(3), N1–Mn1–N1* = 132.5(5), N1–Mn1–N2* = 135.8(3), N2–Mn1–N2* = 141.3(5), N1–C7–N2 = 110.3(8).

general, the metrical parameters associated with **2** are similar to those observed in previously characterized manganese amidinate complexes, although the N–C–N bond angle of the amidinate ligand (110.3(8)°) is substantially smaller than those observed previously (113.5–120.7°).[4,53,54] This is perhaps due to steric interactions between the terphenyl group and the isopropyl groups of the ligand backbone.

The structures of the cobalt (**4**) and nickel (**5**) bis-amidinate species were also determined by X-ray crystallography. The two structures are isomorphic, crystallizing in the monoclinic space group $P2_1/m$. A crystallographic mirror plane cuts through the compounds, rendering the N–C–N planes of the two amidinate ligands perpendicular (interplanar angle = 90°). Also, within each ligand, the terphenyl substituent is perpendicular to the N–C–N binding plane, and hence parallel to the opposite ligand's binding plane. ORTEP diagrams of these are shown below (Figs. 5 (**4**) and 6 (**5**)) and selected metrical parameters are given.

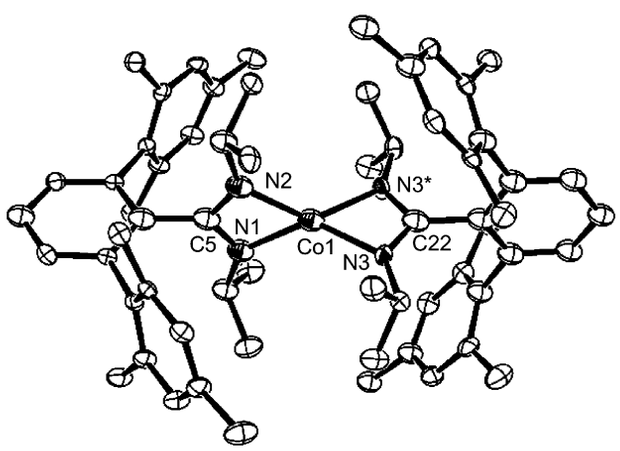

Fig. 5 ORTEP view of $(L_{Me})_2$ Co (**4**) with 50% thermal ellipsoids. Selected bond lengths (Å): Co1–N1 = 1.973(4), Co1–N2 = 1.992(4), Co1–N3 = 1.993(3), N1–C5 = 1.334(6), N2–C5 = 1.329(6), N3–C22 = 1.334(4); bond angles (°): N1–Co1–N2 = 66.0(1), N1–Co1–N3 = 134.6(1), N1–Co1–N3* = 134.6(1), N2–Co1–N3 = 134.8(1), N2–Co1–N3* = 134.8(1), N3–Co1–N3* = 65.9(2), N1–C5–N2 = 108.3(4), N3–C22–N3* = 108.8(4).

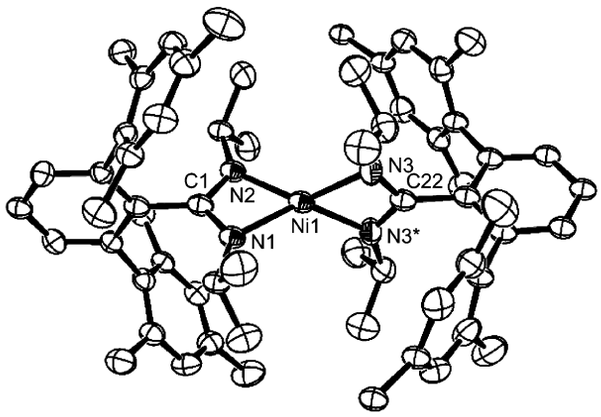

Fig. 6 ORTEP view of $(L_{Me})_2Ni$ (**5**) with 50% thermal ellipsoids. Selected bond lengths (Å): Ni1–N1 = 1.977(2), Ni1–N2 = 1.969(3), Ni1–N3 = 1.972(2), N1–C1 = 1.337(4), N2–C1 = 1.315(4), N3–C22 = 1.325(2); bond angles (°): N1–Ni1–N2 = 66.3(1), N1–Ni1–N3 = 135.40(8), N1–Ni1–N3* = 135.40(8), N2–Ni1–N3 = 133.69(8), N2–Ni1–N3* = 133.69(8), N3–Ni1–N3* = 66.1(1), N1–C1–N2 = 109.0(3), N3–C22–N3* = 108.5(3).

Taking into account the propagation of uncertainty in the determined values,[55] the average bond lengths in **4** are 1.988(2) Å for Co–N and 1.333(3) Å for the N–C of the amidinate backbone. The corresponding values in **5** are 1.972(1) and 1.324(2) Å, respectively. Based on the difference in ionic radii for these two metals (0.69 Å for Ni *versus* 0.72 Å for Co),[56] one would expect to see a corresponding difference of 0.03 Å in M–N bonds in these two species. Though the predicted trend in bond length is followed, the actual bond difference (0.016(2) Å shorter for Ni–N) is less than would be expected. The slight change in the amidinate N–C bond lengths (0.009(4) Å shorter) in the nickel complex may indicate that more electron density remains in the delocalized π-system of the amidinate ligand in **4**. In contrast, the bond angles (N–M–N and N–C–N) are identical within uncertainty levels for these two compounds.

The Co–N bond lengths discussed above are somewhat shorter than those found in the only other previous example of a structurally characterized bis-amidinate Co(II) species {$[FcN(CC_6H_{10})_2]_2Co$, Fc = ferrocenyl} (av. Co–N = 2.011 Å).[57] Bond lengths in other related cobalt(II) species are also generally longer, ranging from 2.065 to 2.259 Å.[58,59] In contrast, the Ni–N bond lengths observed for **5** fall well within the range previously observed for related Ni(II) compounds (1.916–2.141 Å).[4,60]

Mono-amidinate complexes of nickel and copper

As the mono-amidinate transition metal complexes proved to be inaccessible *via* transition metal halide precursors, other transition metal complexes were sought as precursors in these reactions. Specifically, one equivalent of $Ni(acac)_2$ was reacted with the lithium amidinates [L_{Me}–Li(TMEDA) or L_{Bu^t}–Li(TMEDA)] to produce compounds of the form $(L_R)Ni(acac)$ for both the mesityl and the *tert*-butylphenyl substituted ligands (Scheme 2). In both cases, the amidinate ligand displaced one acetylacetonate ligand from the metal complex to form the four-coordinate nickel species. For $[(L_{Me})Ni(acac)]$ (**6**), the product is a green oil at room temperature with a substantially broadened ^1H NMR spectrum, indicative of its paramagnetic nature. The oil was consistently contaminated with a small amount of free-base ligand ($L_{Me}H$), preventing isolation of analytically pure material, and consequently preventing the determination of the magnetic moment (μ_{eff}) for **6**. The best evidence for the formation of **6** was provided by EI mass spectrometry, which showed a molecular ion peak at *m*/*z* 597, consistent with its generation. In contrast, $(L_{Bu^t})Ni(acac)$ (**7**) was a diamagnetic purple solid, which was isolated as a pure crystalline solid. The ^1H NMR spectrum of this species

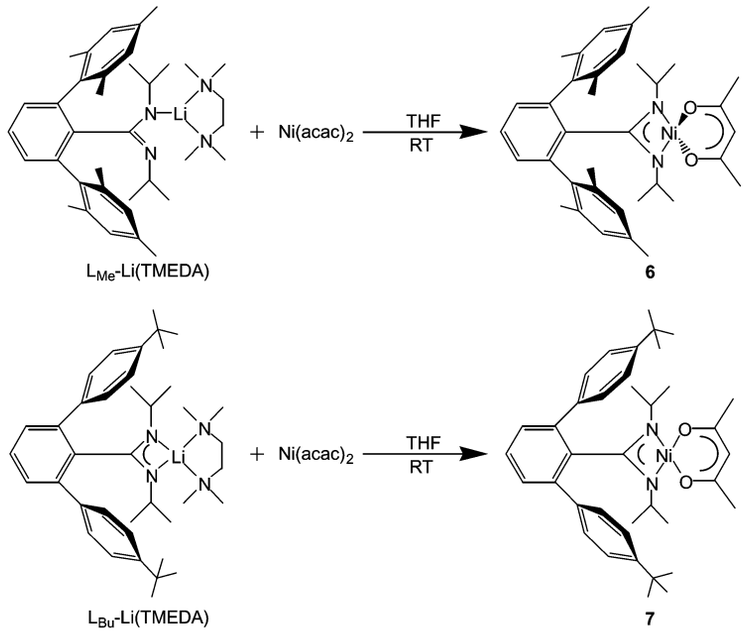

Scheme 2

indicated the presence of one amidinate ligand and one acac ligand with C_{2v} symmetry. The ^{13}C NMR spectrum also showed resonances in agreement with the formulation of **7**, and the mass spectrum again had the expected M^+ ion peak (*m*/*z* 624). Based on these initial data, **6** and **7** were assigned tetrahedral and square planar metal coordination environments, respectively. Both environments are common for previously observed nickel complexes,[61] and the differences observed in these two species may be another indication of the increased steric bulk of the mesityl-substituted amidinate ligand.

The oily nature of **6** made absolute assignment of its geometry difficult, whereas crystallization of **7** from pentane resulted in high-quality crystals of this material. The X-ray structure (Fig. 7) confirms the initially assigned square planar coordination environment (see inset) composed of both amidinate nitrogen atoms and both oxygen atoms from the acac ligand. Though no crystallographically characterized (amidinate)-Ni(acac) compounds exist for comparison, the Ni–N bond lengths of **7** (1.889(3) and 1.882(3) Å) are found to be shorter than those found in related Ni(II) species.[4,60] On the other hand, the Ni–O bond lengths in **7** (1.844(3) and 1.846(3) Å) fall well within the range previously observed for square planar L_2Ni-(acac) species (1.840–1.936 Å).[62–69]

Synthetically, the mono-amidinate complex **7** proved to be a rather poor starting material for the generation of reactive nickel species. The related Cp*Ni(acac) complex has been shown to undergo a variety of substitution reactions, allowing for the generation of a variety of alkyl and aryl complexes by substitution of the acetylacetonate ligand.[70–76] Unfortunately, the reaction of **7** with a wide variety of alkyl, aryl, and amido reagents[77] led only to intractable decomposition mixtures, regardless of the reaction conditions employed.

Another mono-amidinate transition metal complex was synthesized by reaction of the *tert*-butylphenyl substituted amidinate [L_{Bu^t}–Li(TMEDA)] with CuCl in THF (Scheme 3).

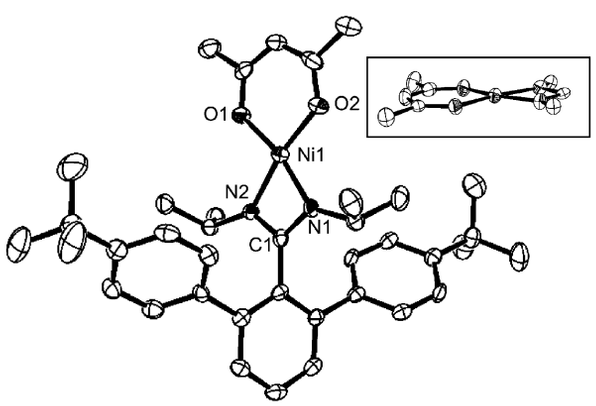

Fig. 7 Side (inset) and top (main) views (ORTEP) of (L_{Bu^t})Ni(acac) (**7**) with 50% thermal ellipsoids. Selected bond lengths (Å): Ni1–N1 = 1.889(3), Ni1–N2 = 1.882(3), Ni1–O1 = 1.846(3), Ni1–O2 = 1.844(3), N1–C1 = 1.326(5), N2–C1 = 1.323(5); bond angles (°): N1–Ni1–N2 = 68.8(1), N1–Ni1–O1 = 165.5(1), N1–Ni1–O2 = 98.0(1), N2–Ni1–O1 = 96.6(1), N2–Ni1–O2 = 166.8(1), O1–Ni1–O2 = 96.6(1), N1–C1–N2 = 107.1(4).

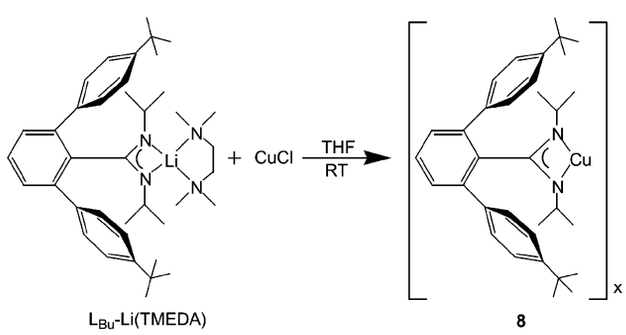

Scheme 3

This simple salt metathesis reaction proceeds with loss of LiCl and formation of [(L_{Bu^t})Cu]$_x$ (**8**) in good yield. The ^1H NMR spectrum of **8** was very simple, showing only seven resonances (all ligand-based) and indicative of a two-fold symmetric amidinate ligand. No coordinated solvent resonances were observed. After thorough washing of the white powder with diethyl ether, **8** was extracted into toluene. Removal of toluene under vacuum yielded a white powder of high purity, as indicated by elemental analysis. Based on these data, **8** was assigned an empirical formula of (L_{Bu^t})Cu. The molecular structure of **8** remains unknown as X-ray quality crystals of this compound proved elusive, but a polymeric or cluster-type arrangement seems likely for this material.

Summary and conclusions

The coordination chemistry of the new sterically-bulky amidinate ligands described recently has been explored, with a focus on the chemistry of the mesityl-substituted ligand. Formation of a series of bis-amidinate complexes deriving from divalent transition metal halides has been presented. Additionally, some mono-amidinate transition metal complexes have been synthesized and characterized. These species demonstrated the useful coordination chemistry of this ligand, but led to little further reaction chemistry.

Acknowledgements

The authors gratefully acknowledge the NSF for funding, the Department of Defense Science and Engineering Graduate (NDSEG) Fellowship Program for fellowship support (JARS), as well as Drs Fred Hollander and Allen Oliver for insightful discussions.

References and notes

1 C. Gerhardt, *Justus Liebigs Ann. Chem.*, 1858, **108**, 219.
2 J. Barker and M. Kilner, *Coord. Chem. Rev.*, 1994, **133**, 219–300.
3 J. R Hagadorn and J. Arnold, *Organometallics*, 1998, **17**, 1355–1368.
4 D. Walther, P. Gebhardt, R. Fischer, U. Kreher and H. Gorls, *Inorg. Chim. Acta*, 1998, **281**, 181–189.
5 P. J. Stewart, A. J. Blake and P. Mountford, *Organometallics*, 1998, **17**, 3271–3281.
6 K. H. Thiele, H. Windisch, F. T. Edelmann, U. Kilimann and M. Z. Noltemeyer, *Z. Anorg. Allg. Chem.*, 1996, **622**, 713–716.
7 J. R. Hagadorn and J. Arnold, *Organometallics*, 1996, **15**, 984–991.
8 J. R. Hagadorn and J. Arnold, *J. Am. Chem. Soc.*, 1996, **118**, 893–894.
9 F. T. Edelmann, *Coord. Chem. Rev.*, 1994, **137**, 403–481.
10 G. Zou and T. Ren, *Inorg. Chim. Acta*, 2000, **304**, 305–308.
11 F. Preuss, M. Scherer, C. Klingshirn, G. Hornung, M. Vogel, W. Frank and G. Z. Reiss, *Z. Naturforsch., Teil B*, 1999, **54**, 1396–1404.
12 R. Gomez, P. Gomez-Sal, A. Martin, A. Nunez, P. A. del Real and P. Royo, *J. Organomet. Chem.*, 1998, **564**, 93–100.
13 D. Y. Dawson and J. Arnold, *Organometallics*, 1997, **16**, 1111–1113.
14 J. R. Hagadorn and J. Arnold, *J. Chem. Soc., Dalton Trans.*, 1997, 3087–3096.
15 P. J. Stewart, A. J. Blake and P. Mountford, *Inorg. Chem.*, 1997, **36**, 1982–1986.
16 C. T. Chen, L. H. Rees, A. R. Cowley and M. L. H. Green, *J. Chem. Soc., Dalton Trans.*, 2001, 1761–1767.
17 K. B. Aubrecht, K. Chang, M. A. Hillmyer and W. B. Tolman, *J. Polym. Sci. Polym. Chem.*, 2001, **39**, 284–293.
18 A. P. Duncan, S. M. Mullins, J. Arnold and R. G. Bergman, *Organometallics*, 2001, **20**, 1808–1819.
19 Z. P. Lu, G. P. A. Yap and D. S. Richeson, *Organometallics*, 2001, **20**, 706–712.
20 S. Bambirra, A. Meetsma, B. Hessen and J. H. Teuben, *Organometallics*, 2001, **20**, 782–785.
21 R. P. Davies, D. J. Linton, P. Schooler, R. Snaith and A. E. H. Wheatley, *Eur. J. Inorg. Chem.*, 2001, 619–622.
22 H. Kondo, Y. Yamaguchi and H. Nagashima, *J. Am. Chem. Soc.*, 2001, **123**, 500–501.
23 D. Doyle, Y. K. Gun'ko, P. B. Hitchcock and M. F. Lappert, *J. Chem. Soc., Dalton Trans.*, 2000, 4093–4097.
24 S. Dagorne, I. A. Guzei, M. P. Coles and R. F. Jordan, *J. Am. Chem. Soc.*, 2000, **122**, 274–289.
25 N. Thirupathi, G. P. A. Yap and D. S. Richeson, *Organometallics*, 2000, **19**, 2573–2579.
26 S. R. Foley, G. P. A. Yap and D. S. Richeson, *J. Chem. Soc., Dalton Trans.*, 2000, **10**, 1663–1668.
27 C. T. Chen, L. H. Doerrer, V. C. Williams and M. L. H. Green, *J. Chem. Soc., Dalton Trans.*, 2000, 967–974.
28 Y. Yamaguchi and H. Nagashima, *Organometallics*, 2000, **19**, 725–727.
29 S. R. Foley, Y. L. Zhou, G. P. A. Yap and D. S. Richeson, *Inorg. Chem.*, 2000, **39**, 924–929.
30 B. Vendemiati, G. Prini, A. Meetsma, B. Hessen, J. H. Teuben and O. Traverso, *Eur. J. Inorg. Chem.*, 2001, 707–711.
31 S. R. Foley, G. P. A. Yap and D. S. Richeson, *Chem. Commun.*, 2000, 1515–1516.
32 E. A. C. Brussee, A. Meetsma, B. Hessen and J. H. Teuben, *Chem. Commun.*, 2000, 497–498.
33 K. M. Carlson-Day, J. L. Eglin and L. T. Smith, *Inorg. Chim. Acta*, 2000, **310**, 282–284.
34 F. A. Cotton, L. M. Daniels, C. A. Murillo and P. Schooler, *J. Chem. Soc., Dalton Trans.*, 2000, 2001–2005.
35 D. D. Ellis and A. L. Spek, *Acta Crystallogr., Sect. C*, 2001, **57**, 147–148.
36 A. E. Guiducci, A. R. Cowley, M. E. G. Skinner and P. Mountford, *J. Chem. Soc., Dalton Trans.*, 2001, 1392–1394.
37 E. W. Abel and S. J. Skittrall, *J. Organomet. Chem.*, 1980, **185**, 391–401.
38 F. Olbrich, G. Schmidt, E. Weiss and U. Behrens, *J. Organomet. Chem.*, 1993, **456**, 299–303.
39 J. A. R. Schmidt and J. Arnold, *J. Chem. Soc., Dalton Transactions*, 2002, 2890–2899.
40 J. A. R. Schmidt and J. Arnold, *Chem. Commun.*, 1999, 2149–2150.
41 H. Chen, R. A. Bartlett, M. M. Olmstead, P. P. Power and S. C. Shoner, *J. Am. Chem. Soc.*, 1990, **112**, 1048–1055.
42 D. F. Evans, *J. Chem. Soc.*, 1959, 2003–2005.
43 L. J. Farrugia, *J. Appl. Crystallogr.*, 1997, **30**, 565.
44 SMART: Area-Detector Software Package, Siemens Industrial Automation, Inc., Madison, WI, 1995.
45 SAINT: SAX Area-Detector Integration Program, V4.024, Siemens Industrial Automation, Inc., Madison, WI, 1995.
46 XPREP: Part of the SHELXTL Crystal Structure Determination Package, V5.03, Siemens Industrial Automation, Inc., Madison, WI, 1995.
47 A. Altomare, G. Cascarano, C. Giacovazzo and A. Guagliardi, *J. Appl. Crystallogr.*, 1993, **26**, 343–350.
48 P. T. Beurskens, G. Admiraal, G. Beurskens, W. P. Bosman, S. Garcia-Granda, R. O. Gould, J. M. M. Smits and C. Smykalla, The DIRDIF Program System, Technical Report of the Crystallography Laboratory, University of Nijmegen, The Netherlands, 1992.
49 teXsan: Crystal Structure Analysis Package, Molecular Structure Corporation, Houston, TX, 1992.
50 D. T. Cromer and J. T. Waber, *International Tables for X-Ray Crystallography*, The Kynoch Press, Birmingham, England, 1974, vol. IV, Table 2.2A.
51 J. A. Ibers and W. C. Hamilton, *Acta Crystallogr.*, 1964, **17**, 781–782.
52 $R = \Sigma||F_o| - |F_c||/\Sigma|F_o|$, $R_w = [(\Sigma w(|F_o| - |F_c|)^2/\Sigma wF_o^2)]^{1/2}$, GOF = $[\Sigma w(|F_o| - |F_c|)^2/(N_o - N_v)]^{1/2}$ where N_o = number of observations and N_v = number of variables, and the weight $w = 4F_o^2/\sigma^2(F_o)^2 = [\sigma^2(F_o) + (pF_o/2)^2]^{-1}$ and p is the factor used to lower the weight of intense reflections.
53 A. Kasani, R. P. K. Babu, K. Feghali, S. Gambarotta, G. P. A. Yap, L. K. Thompson and R. Herbst-Irmer, *Chem. Eur. J.*, 1999, **5**, 577–586.
54 K. Kohler, H. W. Roesky, M. Noltemeyer, H. G. Schmidt, C. Freireerdbrugger and G. M. Sheldrick, *Chem. Ber.*, 1993, **126**, 921–926.
55 D. C. Harris, *Quantitative Chemical Analysis*, 3rd edn., W. H. Freeman and Company, New York, 1991.
56 R. D. Shannon, *Acta Crystallogr., Sect. A*, 1976, **32**, 751–767.
57 J. R. Hagadorn and J. Arnold, *Inorg. Chem.*, 1997, **36**, 132–133.
58 S. Cabaleiro, J. Castro, J. A. Garcia-Vazquez, J. Romero and A. Sousa, *Polyhedron*, 2000, **19**, 1607–1614.
59 F. A. Cotton, C. A. Murillo and X. P. Wang, *Inorg. Chem. Commun.*, 1998, **1**, 281–283.
60 S. Cabaleiro, J. Castro, E. Vazquez-Lopez, J. A. Garcia-Vazquez, J. Romero and A. Sousa, *Polyhedron*, 1999, **18**, 1669–1674.
61 F. A. Cotton and G. Wilkinson, *Advanced Inorganic Chemistry*, 5th edn., John Wiley & Sons, New York, 1988.
62 T. Dohler, H. Gorls and D. Walther, *Chem. Commun.*, 2000, 945–946.
63 R. Schubbe, K. Angermund, G. Fink and R. Goddard, *Macromol. Chem. Phys.*, 1995, **196**, 467–478.
64 M. Maekawa, M. Munakata, T. Kuroda and Y. Nozaka, *Inorg. Chim. Acta*, 1993, **208**, 243–244.
65 M. Maekawa, M. Munakata and T. Kurodasowa, *Inorg. Chim. Acta*, 1994, **227**, 149–151.
66 B. Walther, H. Hartung, M. Maschmeier, U. Baumeister and B. Z. Messbauer, *Z. Anorg. Allg. Chem.*, 1988, **566**, 121–130.
67 J. M. Huggins and R. G. Bergman, *J. Am. Chem. Soc.*, 1979, **101**, 4410–4412.

68 F. A. Cotton, B. A. Frenz and D. L. Hunter, *J. Am. Chem. Soc.*, 1974, **96**, 4820–4825.
69 B. L. Barnett and C. Kruger, *J. Organomet. Chem.*, 1972, **42**, 169–175.
70 J. J. Schneider, U. Denninger, R. Goddard, C. Kruger and C. W. Lehmann, *J. Organomet. Chem.*, 1999, **582**, 188–194.
71 J. J. Schneider, D. Wolf, U. Denninger, R. Goddard and C. Kruger, *J. Organomet. Chem.*, 1999, **579**, 139–146.
72 U. Denninger, J. J. Schneider, G. Wilke, R. Goddard, R. Kromer and C. Kruger, *J. Organomet. Chem.*, 1993, **459**, 349–357.
73 J. Blumel, N. Hertkorn, B. Kanellakopulos, F. H. Kohler, J. Lachmann, G. Muller and F. E. Wagner, *Organometallics*, 1993, **12**, 3896–3905.
74 P. Hudeczek and F. H. Kohler, *Organometallics*, 1992, **11**, 1773–1775.
75 E. E. Bunel, L. Valle and J. M. Manriquez, *Organometallics*, 1985, **4**, 1680–1682.
76 E. E. Bunel, L. Valle, N. L. Jones, P. J. Carroll, M. Gonzalez, N. Munoz and J. M. Manriquez, *Organometallics*, 1988, **7**, 789–791.
77 These reactants included lithium salts of alkyl and aryl amides, aryl oxides, lithium alkyls, and aryl lithium reagents.